

# Can Electromagnetic Information Theory Improve Wireless Systems? A Channel Estimation Example

Jieao Zhu, Xiaofeng Su, Zhongzhichao Wan, Linglong Dai, *Fellow, IEEE*, and Tie Jun Cui, *Fellow, IEEE*

**Abstract**—Electromagnetic information theory (EIT) is an emerging interdisciplinary subject that integrates classical Maxwell electromagnetics and Shannon information theory. The goal of EIT is to uncover the information transmission mechanisms from an electromagnetic (EM) perspective in wireless systems. Existing works on EIT are mainly focused on the analysis of degrees-of-freedom (DoF), system capacity, and characteristics of the electromagnetic channel. However, these works do not clarify how EIT can improve wireless communication systems. To answer this question, in this paper, we provide a novel demonstration of the application of EIT. By integrating EM knowledge into the classical MMSE channel estimator, we observe for the first time that EIT is capable of improving the channel estimation performance. Specifically, the EM knowledge is first encoded into a spatio-temporal correlation function (STCF), which we term as the EM kernel. This EM kernel plays the role of side information to the channel estimator. Since the EM kernel takes the form of Gaussian processes (GP), we propose the EIT-based Gaussian process regression (EIT-GPR) to derive the channel estimations. In addition, since the EM kernel allows parameter tuning, we propose EM kernel learning to fit the EM kernel to channel observations. Simulation results show that the application of EIT to the channel estimator enables it to outperform traditional isotropic MMSE algorithm, thus proving the practical values of EIT.

**Index Terms**—Electromagnetic information theory (EIT), spatio-temporal correlation function (STCF), Gaussian process regression (GPR), kernel learning.

## I. INTRODUCTION

Future sixth-generation (6G) wireless communications [1] embrace emerging technologies, including reconfigurable intelligent surfaces (RISs) [2], cell-free massive multiple-input multiple-output (CF-MIMO) [3], and near-field communications [4]. Although these technologies are expected to be the game changers of designing communication systems, it is believed that profound changes are more likely to originate from re-visiting the fundamental laws that underlie the communication process [5]. The fundamental rules that backbone

wireless communications include electromagnetics (EM theory) and information theory (IT). The integration of these two theories will possibly trigger next-generation communication technologies, which motivates the study of electromagnetic information theory (EIT) [6–9].

EIT is an interdisciplinary subject that integrates deterministic physical theory and statistical mathematical theory to study information transmission mechanisms in spatially continuous electromagnetic (EM) fields [6]. By inheriting thoughts from Maxwell and Shannon, the unified EIT framework is expected to accurately respond to the key performance concerns in communication systems, including the degrees-of-freedom (DoF), information-theoretic capacity, and EM channel properties.

### A. Prior Works

EIT is a dawning concept that have not yet converged to a common belief. The current study of EIT can be divided into two categories: EIT DoF/capacity analysis, and EIT channel analysis.

*EIT DoF and capacity analysis.* The study of EIT DoF and capacity analysis dates back to 1987 [10], where a general scattered EM field observed on a manifold external to a source sphere is first analyzed by a bandlimited approximation analysis. The bandwidth of the approximation bases is termed “spatial bandwidth”. Based on the asymptotic analysis in [10], the authors of [11] further provides rigorous analysis to the DoF of a general scattered field, given that the spatial bandwidth is known in advance. Both of the above works are aimed at evaluating the observed DoF, i.e., the essential dimension of the space composed of all the possible observed field configurations. Since no constraints are imposed on the source of the field, the transmitter has not been considered. To address this problem, a general EIT analysis framework based on solving eigen-systems of the transceiver has been proposed in [12, 13]. By treating the wireless channel as a spatio-temporal linear operator, the capacity is derived via an eigen analysis on this operator. Following this theoretical framework, in [14], a numerical algorithm for solving the eigen-systems is proposed to compute the capacity between transceivers.

*EIT channel analysis.* To better capture the EM properties of the wireless channel, the theoretical framework of EIT has been applied to channel analysis. To describe the random scattering properties of the EM MIMO channel, the authors of [15] expand the EM response by Hankel functions in cylindrical coordinates, and then  $T$ -matrix analysis is performed to accurately compute the information-theoretic quantities associated with the MIMO channel. To further take into consideration the

This work was supported in part by the National Key Research and Development Program of China (Grant No.2020YFB1807201), in part by the National Natural Science Foundation of China (Grant No. 62031019), in part by the U.S National Science Foundation under Grants CCF-1908308 and CNS-2128448, and in part by the National Natural Science Foundation of China under Grant 62288101. (*Corresponding author: Linglong Dai.*)

J. Zhu, X. Su, Z. Wan, and L. Dai are with the Department of Electronic Engineering, Tsinghua University, Beijing 100084, China, and also with the Beijing National Research Center for Information Science and Technology (BNRist), Beijing 100084, China (e-mails: zja21@mails.tsinghua.edu.cn, suxf@tsinghua.edu.cn, wzzc20@mails.tsinghua.edu.cn, daill@tsinghua.edu.cn).

T. J. Cui is with the State Key Laboratory of Millimeter Waves, Southeast University, China (e-mail: tjcui@seu.edu.cn).

EM spatial correlation, the authors of [16, 17] provides a novel Gaussian process (GP) viewpoint of wireless channels. Different from traditional viewpoint that treat the channel as spatio-temporal impulse responses or complex-valued matrices, the channel is represented by a correlated random field that is distributed over the receiving region. This GP representation is derived from the first principles of Maxwell's equations, ensuring its physical consistency. In [18], the authors extend the GP representation in [16, 17] by numerically discretizing the continuous wavenumber domain, and transform the continuous EM channel into the Fourier plane-wave representation. An interesting insight is that the EM channel can be viewed as a circle-shaped linear space-invariant (LSI) filter in the wavenumber domain, which simplifies the subsequent EIT analysis. In recent work of [19], various non-ideal effects, including mutual coupling and correlated fading, are considered to complete the Fourier plane-wave model in [18].

In summary, existing works on EIT are mainly focused on the computation of information-theoretic quantities and the EM-compliant characterization of the wireless channel. These works provide us with insightful viewpoints and novel understandings of the information flow in wireless communication systems. However, they neglect the effect of EIT on designing practical communication systems. Thus, a question naturally arises: *How can we improve wireless communication systems via EIT?*

## B. Our Contributions

To answer this question, in this paper, we provide a simple yet inspiring demonstration of how to apply EIT to communication systems. By integrating EM knowledge into the classical MMSE channel estimation procedure, we observe for the first time that EIT can improve the channel estimation performance of wireless communication systems<sup>1</sup>. The contributions of this paper are summarized as follows.

- We reveal that the prior knowledge about the EM propagation can be accurately represented by a specially constructed spatio-temporal correlation function (STCF), which we term as the *EM kernel*. Since it is directly derived from Maxwell's equations, the EM kernel is both physically interpretable and EM-compliant. Different from the existing STCF analyses, the proposed EM kernel captures the tri-polarized nature and smoothly integrates the angular concentrated properties of the EM fields. Thus, it can better match the real-world wireless propagation environment.
- We further reveal that the EM kernel is equivalent to a Gaussian process. Thus, Gaussian process regression (GPR) algorithms can be applied to fulfill various channel inference tasks, especially the channel estimation problem. Based on this equivalence, we propose the EIT-GPR channel estimation algorithm to fully exploit the side information contained in the EM kernel. Since GPR operates on Gaussian processes, the EIT-GPR algorithm takes the same form as the MMSE estimator, where the

prior covariance is explicitly given by the EM kernel in an interpretable manner.

- Finally, by altering the tunable parameters of the EM kernel, we propose a kernel learning algorithm that dynamically fits the EM kernel to the wireless propagation environment. Performance analysis and numerical experiments verify that, the proposed EIT-GPR channel estimator outperforms traditional isotropic MMSE estimator and compressed sensing estimators, demonstrating that EIT is capable of guiding the design of wireless communication systems.

## C. Organization and Notation

*Organization:* The rest of the paper is organized as follows. In Section II, we introduce the general construction principle of EIT channel models, and formulate the uplink channel estimation problem. In Section III, we first introduce basic mathematical concepts of Gaussian processes (GP), Gaussian random fields (GRF), and the kernel representation. Then, the EM kernel is constructed, together with its extension to fast fading channels, and the analytical properties of the EM kernel is presented. In Section IV, based on the previously constructed EM kernel, we propose the EIT-GPR channel estimation algorithm and the corresponding kernel learning algorithm. In Section V, simulation results are provided for quantifying the performance of our proposed EIT-GPR channel estimation algorithm. Finally, in Section VI, we provide our conclusions followed by promising future research ideas.

*Notation:* Bold uppercase characters  $\mathbf{X}$  denote matrices; bold lowercase characters  $\mathbf{x}$  denote vectors;  $\mathbf{x}(n)$  represents the  $n$ -th component of the vector  $\mathbf{x}$ ;  $\Re\{\cdot\}$  and  $\Im\{\cdot\}$  denote the real and imaginary part of their arguments, respectively; The dot  $\cdot$  denotes the scalar product of two vectors, or the matrix-vector multiplication;  $\partial_k$  is the abbreviation of  $\partial/\partial x^k$ , where  $(x^1, x^2, \dots, x^k, \dots, x^n)$  is a coordinate vector.  $\mathbb{E}[X]$  denotes the mean of random variable  $X(\omega)$ ;  $c$  is the speed of light in a vacuum;  $[N]$  denotes the positive integer set  $\{1, 2, \dots, N\}$ ;  $\mathcal{F}[f(x)]$  denotes the Fourier transform of  $f(x)$ ; For spatial distributions, the Fourier basis is  $e^{i\mathbf{k}\cdot\mathbf{x}}$ , and for temporal signals, the Fourier basis is  $e^{-i\omega t}$ ; For  $\mathbf{x} \in \mathbb{C}^n$  or  $\mathbb{R}^n$ ,  $|\mathbf{x}|$  denotes the pseudo-norm  $\sqrt{\mathbf{x}^T \mathbf{x}} \in \mathbb{C}$ ,  $\|\mathbf{x}\|$  denotes the standard vector 2-norm  $\sqrt{\mathbf{x}^H \mathbf{x}} \in \mathbb{R}_{\geq 0}$ ;  $\hat{\mathbf{x}}$  represents  $\mathbf{x}/|\mathbf{x}|$  unless otherwise stated;  $\nabla$  is the gradient operator, and  $\nabla \times$  is the curl operator;  $J_\nu(x)$  is the  $\nu$ th-order Bessel function of the first kind;  $\mathbb{S}_+^n$  is the collection of all the complex semi-positive definite matrices.  $S^n$  denotes the  $n$ -dimensional unit sphere embedded in  $\mathbb{R}^{n+1}$ .

## II. SYSTEM MODELS AND PROBLEM FORMULATION

In this section, we will first review the principles of EIT channel analysis, where different kinds of channel models and their distinct roles in designing channel estimation algorithms are summarized. Then, the uplink channel estimation problem is formulated in a probabilistic manner.

<sup>1</sup>Simulation codes will be provided to reproduce the results in this paper: <http://oa.ee.tsinghua.edu.cn/dailinglong/publications/publications.html>.

### A. Channel Models

Channel models can be divided into two main categories according to their applications. The first kind is the simulation channel model (SCM), which accurately models the EM propagation channel for simulation purposes [20, 21], among which the most representative example is the TR 38.901 model [20]. However, this kind of SCM model is usually over-parameterized, i.e., it contains enormous parameters to ensure model accuracy, whose number of parameters is usually greater than the intrinsic degrees of freedom (DoF) of the channel. Due to large numbers of redundant parameters, SCMs cannot be directly applied to designing channel estimation algorithms.

To solve the complexity curse of SCMs, simpler models [22, 23] are usually adopted to enable computationally feasible channel estimation, where one of the most often applied model is the Saleh-Valenzuela channel model (SV model, [23]). We name these simpler models as computational channel models (CCMs). CCMs strike a balance between model accuracy and model complexity. Thus, properly constructing CCMs is of practical importance in designing efficient channel estimation algorithms.

An important question is the evaluation of a CCM, i.e., how can we know that a CCM is favorable? To answer this question, let us denote the generative SCM as  $p(\mathbf{h})$ , where  $\mathbf{h}$  is some channel vector<sup>2</sup>, and the probability measure  $p$  assigns a probability value to each channel realization  $\mathbf{h}$ . The true distribution  $p$  is usually unknown due to the complexity and dynamicity of the wireless propagation environment. This absence of the true SCM probability  $p$  motivates the construction of an approximated CCM probability  $q$ , which can be found via

$$q^* = \arg \min_q (\lambda D_{\text{KL}}(q||p) + (1 - \lambda)H(q)), \lambda \in [0, 1], \quad (1)$$

where  $D_{\text{KL}}(\cdot||\cdot)$  denotes the KL divergence between two distributions [24], and  $H(\cdot)$  is the entropy functional. In the above equation (1), the first term  $D_{\text{KL}}(q||p)$  corresponds to the accuracy of the surrogate model  $q$ , and the second term  $H(q)$  measures the model complexity. The parameter  $\lambda \in [0, 1]$  achieves a trade-off between model accuracy and complexity.

In this paper, we aim to construct an electromagnetic information theory (EIT)-based CCM  $q(\cdot)$ . Compared to existing channel models, the proposed model is explainable in the framework of EM theory, and it will exhibit better channel inference performance due to the *side information* [25] provided by  $q$ .

### B. Uplink Channel Estimation

To demonstrate the effectiveness of the proposed EIT-based CCM, we apply it to the uplink channel estimation problem in a narrowband system. Assume an  $N_{\text{BS}}$ -antenna base station (BS) with fully digital precoding, where each antenna is

connected to a dedicated radio-frequency (RF) chain. The uplink signal model is

$$\mathbf{y} = \mathbf{h} + \mathbf{n}, \quad (2)$$

where  $\mathbf{y} \in \mathbb{C}^{N_{\text{BS}} \times 1}$  is the BS received pilots,  $\mathbf{h} \in \mathbb{C}^{N_{\text{BS}} \times 1}$  is the normalized channel vector satisfying  $\mathbb{E}[\|\mathbf{h}\|^2] = N_{\text{BS}}$ , and  $\mathbf{n}$  is the complex-valued additive white Gaussian noise (AWGN) with zero mean and covariance  $\gamma^{-1}\mathbf{I}_{N_{\text{BS}}}$ . The symbol  $\gamma$  represents the BS's receive signal-to-noise ratio (SNR) during uplink channel estimation.

The goal of uplink channel estimation is to retrieve the unknown channel  $\mathbf{h}$  from the received pilot signal  $\mathbf{y}$ . The theoretically optimal channel estimator for the signal model (2) is the minimum mean-square error (MMSE) estimator, which is given by

$$\hat{\mathbf{h}}^{\text{MMSE}} := \mathbb{E}[\mathbf{h}|\mathbf{y}] \stackrel{(a)}{=} \mathbf{R}_{\mathbf{h}} \left( \mathbf{R}_{\mathbf{h}} + \frac{1}{\gamma} \mathbf{I} \right)^{-1} \mathbf{y}, \quad (3)$$

where (a) holds when  $\mathbf{h}$  is both zero-mean Gaussian distributed and independent of  $\mathbf{n}$ . The covariance matrix  $\mathbf{R}_{\mathbf{h}} \in \mathbb{S}_+^{N_{\text{BS}}}$  is the prior covariance of the channel vector  $\mathbf{h}$ . Usually, the channel covariance cannot be obtained *a priori*, which prohibits the application of the optimal MMSE estimator. To solve this problem, statistical methods are proposed in the literature, where previous channel observations are exploited to compute the channel covariance [26]. However, these methods require extra historical channel recordings, which brings additional memory consumption and slowed down computation. Besides, the statistically computed channel covariance is purely empirical and thus physically unexplainable, which limits its application to other channel inference tasks.

## III. THE PROPOSED EM KERNEL

In this section, we will first introduce the EIT channel modeling method based on Gaussian Random Fields (GRFs). It is proven in Section III-A that GRFs are uniquely determined by their kernels. Based on this observation, in Subsection III-B, we propose a novel EM kernel that can capture the EM propagation characteristics. The properties of the proposed EM kernel are analyzed in detail in Subsection III-D.

### A. Gaussian Random Fields and the Kernel Method

Random fields are mathematical objects that can naturally characterize the random properties of wireless channels, independent of the antenna geometry. Let  $h(\mathbf{x}) : D \rightarrow \mathbb{C}$  be a Lebesgue-measurable function that takes in values from its domain  $D$ , and gives out complex values. Since this function is deterministic, it cannot capture the random fading characteristics of wireless channels. To address this defect, we assign an extra probabilistic measure to the function  $h$ , taking all the possible functions into consideration. This means that the function  $h$  is “upgraded” into a bi-variate function

$$h(\mathbf{x}, \omega) : D \times \Omega \rightarrow \mathbb{C}, \quad (4)$$

where  $\omega \in \Omega$  is the probabilistic sample point, and  $\Omega$  is the sample space. Since the function  $h$  lives in a random sample space  $\Omega$  with multi-dimensional domain  $D \subset \mathbb{R}^n$ , we

<sup>2</sup>We will not dive deep into the definition here, since this probabilistic representation  $p(\mathbf{h})$  is general enough to denote any type of channel distributions.

name it as a  $n$ -dimensional random field. Furthermore, if we assume that for arbitrary  $K$  points  $\{\mathbf{x}_k\}_{k=1}^K \subset D$ , the joint distribution of  $K$  function values  $(h(\mathbf{x}_1), h(\mathbf{x}_2), \dots, h(\mathbf{x}_K))$  follows a multi-variate Gaussian distribution, then the random field  $h$  is a Gaussian random field (GRF)<sup>3</sup>, denoted as  $h(\mathbf{x}) \sim \mathcal{GRF}(m(\mathbf{x}), k(\mathbf{x}, \mathbf{x}'))$ . Similar to multi-variate Gaussian distributions, the probability measure of GRFs are completely determined by their mean functions and autocorrelation functions

$$\begin{aligned} m_h(\mathbf{x}) &:= \mathbb{E}[h(\mathbf{x})], \\ R_h(\mathbf{x}; \mathbf{x}') &:= \mathbb{E}[h(\mathbf{x})h^*(\mathbf{x}')]. \end{aligned} \quad (5)$$

The autocorrelation function  $R_h : D \times D \rightarrow \mathbb{C}$  is usually called the *kernel* of the GRF  $h$ . Note that not all of the bi-variate functions are kernels of some GRF. To represent some GRF, the kernel function must be positive semi-definite [27].

In order to model the wireless channel with GRFs, some restrictions must be imposed on the GRF kernel to make the generated random functions  $h(\mathbf{x}, t, \omega)$  subject to the EM propagation constraints. Suppose we want to model the electric field distribution by a GRF  $h(\mathbf{x}, t)$ , where  $(\mathbf{x}, t) \in \mathbb{R}^4$  is a four-dimensional vector<sup>4</sup>. It can be derived from Maxwell's equations that, a time-harmonic electric field  $\mathbf{E}(\mathbf{x}, t) = \mathbf{E}(x_1, x_2, x_3, t) : \mathbb{R}^4 \rightarrow \mathbb{C}^3$  with fixed frequency  $f_0$  satisfies the Helmholtz equation

$$\nabla^2 \mathbf{E} + k_0^2 \mathbf{E} = \mathbf{0}, \quad (6)$$

where  $k_0 = 2\pi f_0/c$  is the wavenumber. By applying the Helmholtz operator to the random field  $h(\mathbf{x}, \omega)$  for each  $\omega$  and taking the probabilistic average, we obtain from (5) that

$$(\nabla^2 + k_0^2)R_h(\mathbf{x}; \mathbf{x}') = 0. \quad (7)$$

**Remark 1.** The necessary condition of a given autocorrelation function to be EM-compliant is Eqn. (7).

Furthermore, if the GRF is vector-valued, then its autocorrelation is defined as  $\mathbf{R}_{\mathbf{E}}(\mathbf{x}; \mathbf{x}') = \mathbb{E}[\mathbf{E}(\mathbf{x})\mathbf{E}(\mathbf{x}')^H]$ . In this definition, the autocorrelation function is upgraded to an autocorrelation matrix  $\mathbf{R}_{\mathbf{E}} \in \mathbb{C}^{3 \times 3}$ , where the matrix element  $(\mathbf{R}_{\mathbf{E}})_{ij}$ ,  $i, j \in \{1, 2, 3\}$  or  $i, j \in \{x, y, z\}$  represents the cross-polarized correlation between polarization  $i$  and  $j$ . Although this matrix-valued autocorrelation seems cumbersome, it is possible to construct greatly simplified mathematical expressions by making physically reasonable assumptions, which will be presented in the next subsection.

### B. Construction of the EM Kernel

We will construct a novel computational channel model based on EIT and the above matrix-valued GRF theory. To meet these requirements, we begin by rethinking the fundamental EM laws beneath all kinds of communication systems. The proposed channel model should be both deeply rooted in EM theory and highly applicable to existing channel estimation algorithms. Thanks to the GRF framework, a feasible

approach is to specify the autocorrelation matrix  $\mathbf{R}$  of the “channel field”. In this way, we can encode the EM knowledge into the autocorrelation function of the channel response. From a signal processing viewpoint, this is equivalent to specifying the correlation matrix of the channel vector [28].

Motivated by this idea, we start by evaluating the EM channel correlation at two separate points located in the receiver's region  $\mathbf{x}, \mathbf{x}' \in V_R \subset \mathbb{R}^3$ . By assuming unit transmission power, the channel from the source to receiver is proportional to the received electric field observed at  $\mathbf{x}$ , i.e.,  $\mathbf{E}(\mathbf{x}) \in \mathbb{C}^3$ , and the definition of  $\mathbf{E}(\mathbf{x}')$  is similar. Notice that our goal is to evaluate the correlation matrix  $\mathbf{R}(\mathbf{x}; \mathbf{x}') := \mathbb{E}[\mathbf{E}(\mathbf{x})\mathbf{E}^H(\mathbf{x}')] with some reasonable assumption on the surrounding scattering conditions. Since an arbitrary EM field configuration can be accurately represented by an infinite superposition of planar waves with complex amplitude  $\mathbf{E}_0(\boldsymbol{\kappa})$ , i.e.,$

$$\mathbf{E}(\mathbf{x}) = \frac{1}{(2\pi)^3} \int_{\mathbb{R}^3} \mathbf{E}_0(\boldsymbol{\kappa}) e^{i\boldsymbol{\kappa} \cdot \mathbf{x}} d^3 \boldsymbol{\kappa}, \quad (8)$$

we know immediately that the correlation  $\mathbf{R}(\mathbf{x}, \mathbf{x}')$  depends intrinsically on the statistics of the planar wave component  $\mathbf{E}_0(\boldsymbol{\kappa})$ . By assuming an independent complex Gaussian amplitude of this component and noticing  $\boldsymbol{\kappa} \cdot \mathbf{E}_0 = 0$ , we obtain the correlation matrix (up to a constant factor) as

$$\mathbf{R}(\mathbf{x}; \mathbf{x}') \propto \int_{\hat{\boldsymbol{\kappa}} \in S^2} (\mathbf{I} - \hat{\boldsymbol{\kappa}}\hat{\boldsymbol{\kappa}}^T) e^{ik_0 \hat{\boldsymbol{\kappa}} \cdot (\mathbf{x} - \mathbf{x}')} \nu(S) dS, \quad (9)$$

where the integral is taken over the surface of the unit sphere  $S^2$ ,  $\hat{\boldsymbol{\kappa}}$  is the unit radius vector, and  $k_0 = 2\pi/\lambda_0$  is the wavenumber.

**Remark 2.** The integrand  $\mathbf{I} - \hat{\boldsymbol{\kappa}}\hat{\boldsymbol{\kappa}}^T$  automatically ensures the Fourier transformed version of Gauss law for electric fields  $\nabla \cdot \mathbf{E} = 0$ , i.e.,  $i\boldsymbol{\kappa} \cdot \mathbf{E}_0 = 0$ .

By further assuming isotropic EM incidence, i.e.,  $\nu(S) \equiv 1$ , we directly compute the closed-form formula of  $\mathbf{R}(\mathbf{x}; \mathbf{x}')$  to be [29]

$$\begin{aligned} \mathbf{R}(\mathbf{x}; \mathbf{x}') &:= \mathbb{E}[\mathbf{E}(\mathbf{x})\mathbf{E}^H(\mathbf{x}')] \\ &= \frac{\sigma^2}{8} (f_0(k_0 r) + f_2(k_0 r)) \mathbf{I}_3 \\ &\quad + \frac{\sigma^2}{8} (f_0(k_0 r) - 3f_2(k_0 r)) \hat{\mathbf{r}}\hat{\mathbf{r}}^T, \end{aligned} \quad (10)$$

where the radius vector is defined as  $\mathbf{r} = \mathbf{x} - \mathbf{x}'$ ,  $r = \sqrt{\mathbf{r}^T \mathbf{r}}$ ,  $\hat{\mathbf{r}} = \mathbf{r}/r$ , and the single-variable analytic function  $f_n(\beta)$  is given by [30]

$$f_n(\beta) = \int_{-1}^1 x^n e^{i\beta x} dx, \quad (11)$$

which is the (inverse) Fourier transform of the truncated power function  $x^n \mathbb{1}_{[-1,1]}(x)$ .

**Remark 3.** The EM autocorrelation (10) is expressed in an explicit form under the assumption  $\nu = 1$ , describing the correlation factor between a pair of antennas located in arbitrary positions  $\mathbf{x}, \mathbf{x}'$  and arbitrary orientations. Given the unit polarization vector  $\mathbf{p}, \mathbf{p}' \in S^2 \subset \mathbb{R}^3$ , the correlation of the measured channel responses of this pair of antennas is

<sup>3</sup>GRFs are equivalent with multi-dimensional Gaussian processes.

<sup>4</sup>This four-dimensional vector is called the spacetime coordinate in Einstein's special and general relativity.

given by  $\mathbf{p}^\top \mathbf{R} \mathbf{p}' \in \mathbb{C}$ .

**Remark 4.** The EM autocorrelation (10) is invariant under spatial translations, since the correlation values only depend on the spatial displacement vector  $\mathbf{r} = \mathbf{x} - \mathbf{x}'$ . Thus, Eqn. (10) can be written in a more compact form  $\mathbf{R}(\mathbf{r})$ .

Note that the foregoing coefficient  $\sigma^2/8$  in (10) ensures the channel energy normalization condition  $\text{tr}(\mathbf{R}(\mathbf{x}; \mathbf{x})) = \sigma^2, \forall \mathbf{x} \in \mathbb{R}^3$ . Interestingly, although the correlation model (10) is obtained under isotropic scattering conditions, it can be easily extended to the non-isotropic case by the following simple variable substitution:

$$\mathbf{r} \rightarrow \mathbf{r} - i\boldsymbol{\mu}/k_0. \quad (12)$$

This is due to the fact that replacing  $\mathbf{r}$  by  $\mathbf{r} - i\boldsymbol{\mu}/k_0$  is equivalent to introducing an exponential modulation factor  $\nu = e^{\hat{\mathbf{r}} \cdot \boldsymbol{\mu}}$  to the integrand in (9). This modulation factor  $\nu$  introduces non-isotropic properties to the incoming EM waves by assigning larger weights to the directions parallel to  $\boldsymbol{\mu}$ , as well as suppressing the directions anti-parallel to  $\boldsymbol{\mu}$ . It is also known as the von Mises-Fisher (vMF) distribution [31]. Thus, we call  $\boldsymbol{\mu} \in \mathbb{R}^3$  the *concentration parameter*. The direction of  $\boldsymbol{\mu}$  indicates the EM-concentrated direction, and the norm  $\|\boldsymbol{\mu}\|$  is the concentration. The variable substitution in (12) is well-known as the analytic continuation technique [32], where the domain of a real-variable function is extended to complex values and maintains favourable analytic properties such as complex differentiability and the validity of closed-form expressions. This analytic continuation process is analogous to the extension from Fourier transforms to Laplace transforms, where Fourier harmonic integral kernel  $e^{-i\omega t}, \omega \in \mathbb{R}$  is replaced by its analytic continuation  $e^{-st}, s \in \mathbb{C}$ . By working in the complex domain, the concentration property can be seamlessly integrated into the existing correlation model (9).

**Remark 5.** It can be observed in (12) that the real part of the complex displacement vector  $\mathbf{r}$  means spatial separation of different receivers, while the imaginary part of  $\mathbf{r}$ , i.e.,  $\boldsymbol{\mu}$ , corresponds to the directional concentration of incoming EM waves. By analytic continuation, these two different physical quantities can be treated equally as a single complex vector.

Despite the favorable mathematical properties brought by (12), the introduction of a non-constant modulation factor  $\nu$  also violates the energy normalization condition  $\text{tr}(\mathbf{R}) = \sigma^2$ . Thus, we need to introduce an additional normalization factor

$$C(\mu) = \int_{S^2} \nu(S, \boldsymbol{\mu}) dS = \sinh(\mu)/\mu, \quad (13)$$

where  $\mu = \|\boldsymbol{\mu}\| \in \mathbb{R}_+$ , and  $\nu(S, \boldsymbol{\mu}) = e^{\hat{\mathbf{r}} \cdot \boldsymbol{\mu}}$ . By applying this normalization factor, the EM correlation is written as

$$\mathbf{K}_{\text{EM}}(\mathbf{x}; \mathbf{x}') = \frac{\sigma^2}{C(\|\boldsymbol{\mu}\|)} \boldsymbol{\Sigma}(k_0 \mathbf{z}), \quad (14)$$

where  $\mathbf{K}_{\text{EM}}: \mathbb{C}^3 \rightarrow \mathbb{C}^{3 \times 3}$  is called the electromagnetic kernel, i.e., the *EM kernel*. In the above expression of the EM kernel, the complex displacement vector is defined as  $\mathbf{z} = (\mathbf{x} - \mathbf{x}') - i\boldsymbol{\mu}/k_0 \in \mathbb{C}^3$ , and the matrix-valued correlation function that

appears above is written as

$$\begin{aligned} \boldsymbol{\Sigma}(\mathbf{w}) = & \frac{1}{8} (f_0(|\mathbf{w}|) + f_2(|\mathbf{w}|)) \mathbf{I}_3 \\ & + \frac{1}{8} (f_0(|\mathbf{w}|) - 3f_2(|\mathbf{w}|)) \hat{\mathbf{w}} \hat{\mathbf{w}}^\top. \end{aligned} \quad (15)$$

### C. Extension to Fast Fading Channels

Channel fading is the culprit of communication outages. Among the four types of channel fading, i.e., large-scale, small-scale, frequency-selective and time-selective fast fading, the last two are the most difficult to combat due to their rapid changing properties. The proposed EM kernel is capable of explaining the spatial correlation of small-scale fading in an EM-compliant manner. To further describe the fast temporal channel variations, the spatial correlation function  $\mathbf{R}(\mathbf{x}; \mathbf{x}')$  should be extended into a spatio-temporal correlation function (STCF), which is expressed as  $\mathbf{R}(\mathbf{x}, t; \mathbf{x}', t')$ . Generally, this function has no analytical form.

Fortunately, by assuming a von Mises density in the wavenumber domain, the analytical expression of the STCF with additional temporal variable  $t$  can be obtained by the same analytic continuation technique. In fact, by introducing a velocity vector  $\mathbf{v} \in \mathbb{R}^3$ , we can incorporate time selectiveness, i.e., Doppler shift, into the proposed EM kernel. The correlation function is then augmented to support space-time variables  $(\mathbf{x}, t) \in \mathbb{R}^4$ , i.e.,

$$\mathbf{K}_{\text{EM}}(\mathbf{x}, t; \mathbf{x}', t') = \frac{\sigma^2}{C(\|\boldsymbol{\mu}\|)} \boldsymbol{\Sigma}(k_0 \mathbf{z}), \quad (16)$$

where  $\mathbf{z} = \mathbf{r} + \mathbf{v}(t - t') - i\boldsymbol{\mu}/k_0 \in \mathbb{C}^3$ .

**Remark 6.** In Eqn. (16), it can be observed that the Doppler effect caused by the motion of the receiving antenna array is equivalent to an antenna displacement  $\mathbf{v}(t - t')$ . This conclusion is as expected, since the Doppler frequency shift is caused by the motion of the observer. In other words, the STCF (16) automatically incorporates the Doppler effect.

### D. Properties of the EM Kernel

Since the EM kernel  $\mathbf{K}_{\text{EM}}: \mathbb{R}^4 \rightarrow \mathbb{C}^{3 \times 3}$  is a four-dimensional complex-argument matrix-valued function, we study the mathematical properties from two aspects: (1)  $\mathbf{K}_{\text{EM}}$  as a function of the real argument, i.e., the spatial displacement vector  $\mathbf{r} = \mathbf{x} - \mathbf{x}'$  and the time difference  $\Delta t = t - t'$ ; (2)  $\mathbf{K}$  as a function of the imaginary argument, i.e., the concentration parameter  $\boldsymbol{\mu}$ .

(1) *The EM kernel v.s. real displacement  $\mathbf{r}$ .* First, we assume  $\Delta t = 0$ , i.e., we focus on the channel correlation between different antennas at the same instant. Since the real displacement vector  $\mathbf{r}$  describes the vector pointing from the reference antenna to the observation antenna, the value of the EM kernel is exactly the channel correlation coefficient between the reference antenna and the observation antenna, up to a constant scaling. These correlation coefficients are especially instructive in channel prediction tasks [33], where only partial or previous channel coefficients are observable but complete channel matrices are required for subsequent signal

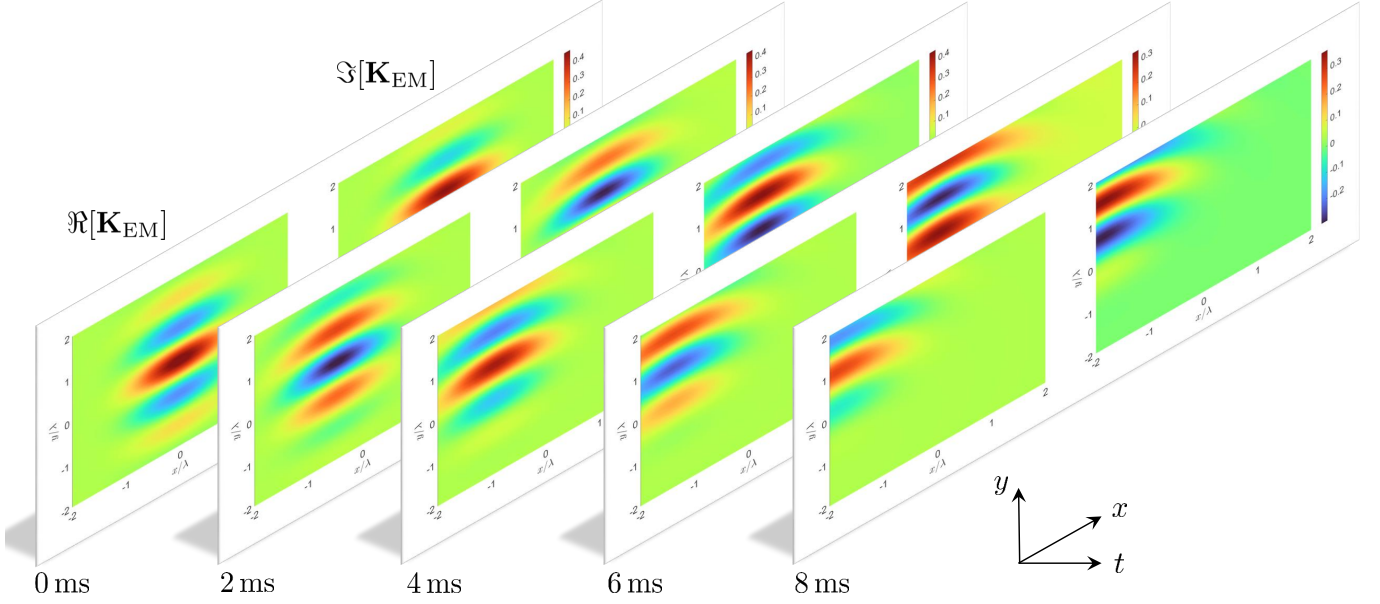


Fig. 1. Slice chart of the space-time EM kernel  $\mathbf{K}_{\text{EM}}(\mathbf{r}, t)$ , where  $\mathbf{r} = (x, y, z)$ . The real part and the imaginary part of the EM kernel are shown in two groups of figures.

processing. By evaluating the EM kernel as a function of  $\mathbf{r}$ , a prior knowledge about the spatial correlation coefficients can be readily obtained.

Second, we fix  $\mathbf{r} = \mathbf{0}$ , and allow the time difference  $\Delta t$  to vary. In this case, the EM kernel describes the temporal correlation of the channel. It is worth noting that, the variation of the complex channel gain is attributed to the relative movement of the transmitter and the receiver. A classical temporal correlation model is the Jake's model (or Clarke's model) [34, 35]. In this model, the temporal channel correlation is expressed as

$$c_h(t, t') := \mathbb{E}[h(t)h^*(t')] = \sigma_h^2 J_0(2\pi v(t - t')/\lambda), \quad (17)$$

where  $v$  [m/s] is the velocity of the moving receiver,  $\lambda$  [m] is the operating wavelength, and  $\sigma_h^2$  is the mean channel energy. The Jake's model is derived in a scalar wave 2-D settings with isotropic scattering, i.e., the incoming wave has no directivity [17]. This model is exact in the scalar wave isotropic environment, however, it neglects the vector nature of EM fields. In contrast, the vector property is well-captured by the proposed EM kernel (16).

To summarize the above spatial and temporal discussions about the EM kernel, we illustrate the kernel as a function of the spacetime 4-vector  $(\mathbf{x}, t)$  in Fig. 1. In the simulation, the concentration vector  $\boldsymbol{\mu} = [0, 10, 10]^T$ , and the user's velocity is  $\mathbf{v} = [20, 0, 20]^T$  m/s with  $y$ -polarized antennas. It can be observed from Fig. 1 that: (a) The spatial correlation peaks at the origin  $\mathbf{r} = \mathbf{0}$ ,  $\Delta t = 0$ , and decays with oscillation as  $\mathbf{r} \rightarrow \infty$ ,  $\Delta t \rightarrow \infty$ ; (b) The velocity  $\mathbf{v}$  causes a translation of the covariance in the spatial domain. The first observation is consistent with existing channel correlation models in the literature [17, 19, 35, 36], but the second observation has not been revealed before. In fact, the temporal channel variation are usually attributed to Doppler frequency shift in the liter-

ature, but intrinsically it is caused by the movement of the receiving antenna. Thus, a unified EM model that combines the velocity  $\mathbf{v}$  with the displacement  $\mathbf{r}$  is self-complete, i.e., no additional Doppler models are needed.

(2) *The EM kernel v.s. imaginary displacement  $\boldsymbol{\mu}$ .* Unlike the previously discussed  $\mathbf{r}$ , the concentration parameter  $\boldsymbol{\mu}$  is often neglected in existing works. From the analytic continuation derivation of (14) we can observe that, the introduction of  $\boldsymbol{\mu}$  is equivalent to an additional spatial non-istropic factor  $\nu = e^{\hat{\mathbf{r}} \cdot \boldsymbol{\mu}}$ . This factor  $\nu$  is mathematically equivalent to a 3D vMF angular distribution of the impinging waves [17, 18]. However, the authors of [18] does not realize the analytic continuation technique, and thus they do not provide a closed-form expression of the correlation function. The existence of such a closed-form expression avoids the complicated evaluation of the coupling coefficients in the Fourier plane-wave domain, thus enabling low-complexity parameter fitting without computing massive summations.

Another important observation is that the imaginary displacement  $\boldsymbol{\mu}$  controls the complexity of the EM kernel. Due to spherical symmetry, the model complexity is independent of the direction  $\hat{\boldsymbol{\mu}} := \boldsymbol{\mu}/\|\boldsymbol{\mu}\|$ , but it depends on the scalar concentration  $\mu := \|\boldsymbol{\mu}\|$ . Fig. 2 shows the relationship between model entropy and the concentration parameter  $\mu$ , with  $\hat{\boldsymbol{\mu}} = [0, 1, 1]^T/\sqrt{2}$ ,  $N_{\text{BS}} = 12$ , and various antenna spacings  $d$ . The model (differential) entropy  $H(\mu)$  is defined as  $\log \det(\pi e \mathbf{K})$  [37], where  $\mathbf{K} \in \mathbb{S}_+^{N_{\text{BS}}}$  is sampled from the EM kernel  $\mathbf{K}_{\text{EM}}$  with spatial spacing  $d$ . From Fig. 2, it can be concluded that the proposed EM kernel becomes less complicated, i.e., contains less parameters, when  $\mu \rightarrow \infty$ . This is because highly concentrated impinging waves are closer to planar waves, while planar waves are the simplest field configurations that contain the least number of parameters.



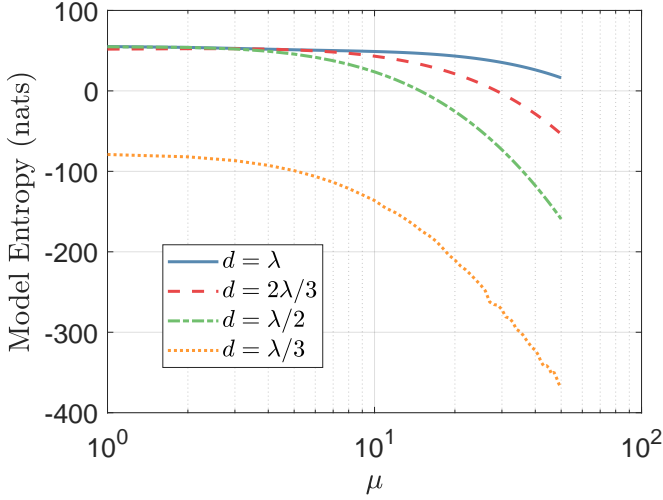


Fig. 2. Kernel entropy as a function of the concentration parameter  $\mu$  with different antenna spacing.

#### IV. PROPOSED EIT-GPR CHANNEL ESTIMATION ALGORITHM

In this section, we will propose a novel GPR-inspired channel estimator based on the proposed EM kernel.

##### A. Gaussian Process Regression (GPR)

Gaussian process regression (GPR) methods can provide prediction from a GRF prior and the observed data [27]. The GRF is specified by  $f(x) \sim \mathcal{GRF}(m(x), k(x, x'))$ , and the data  $y_i$  is observed on a set of points  $\{x_i\}_{i=1}^N \subset D$ , satisfying  $y_i = f(x_i) + \epsilon_i$ . The observation noise  $\epsilon_i \stackrel{\text{i.i.d.}}{\sim} \mathcal{CN}(0, \sigma_\epsilon^2)$ . The objective of GPR is to generate prediction  $f_* := f(x_*)$  at any  $x_* \in D$ , given the observed data  $\mathbf{y} = \{y_i\}_{i=1}^N$ .

Since the mean and covariance of the joint observation-prediction vector  $\mathbf{z} = (y_1, y_2, \dots, y_N, f_*)^T \in \mathbb{C}^{N+1}$  is determined as

$$\begin{aligned} \mathbf{m} &= (m(x_1), m(x_2), \dots, m(x_N), m(x_*))^T, \\ \mathbf{C} &= \begin{bmatrix} k(x_1, x_1) & k(x_1, x_2) & \cdots & k(x_1, x_*) \\ k(x_2, x_1) & k(x_2, x_2) & \cdots & k(x_2, x_*) \\ \vdots & \vdots & \ddots & \vdots \\ k(x_N, x_1) & k(x_N, x_2) & \cdots & k(x_N, x_*) \\ k(x_*, x_1) & k(x_*, x_2) & \cdots & k(x_*, x_*) \end{bmatrix}, \end{aligned} \quad (18)$$

thus by applying the Gaussian posterior formula [38], we obtain

$$\begin{aligned} m_{f_*|\mathbf{y}} &= m(x_*) + \mathbf{k}^H (\mathbf{C}_\mathbf{y})^{-1} (\mathbf{y} - \mathbf{m}_\mathbf{y}) \in \mathbb{C}, \\ c_{f_*|\mathbf{y}} &= k(x_*, x_*) - \mathbf{k}^H (\mathbf{C}_\mathbf{y})^{-1} \mathbf{k} \in \mathbb{R}_+, \end{aligned} \quad (19)$$

where

$$\begin{aligned} \mathbf{k} &= \mathbf{C}(1 : N, N+1) \in \mathbb{C}^{N \times 1}, \\ \mathbf{C}_\mathbf{y} &= \mathbf{C}(1 : N, 1 : N) + \sigma_\epsilon^2 \mathbf{I}_N \in \mathbb{C}^{N \times N}. \end{aligned} \quad (20)$$

The predictive mean, i.e., the regression result, is given by  $m_{f_*|\mathbf{y}}$  in (19), together with the predictive variance  $c_{f_*|\mathbf{y}}$ . Since the prior distribution is Gaussian, the Bayesian GPR estimator coincides exactly with the maximum *a priori* (MAP)

estimator and the maximum likelihood (ML) estimator. Due to its Bayesian optimality, the GPR predictor has been widely applied to various high-precision inference tasks including curve fitting, pattern recognition and data interpolation. Furthermore, in addition to the Bayesian optimality, the wide application of GPR is also attributed its capability of tuning the kernel  $k(x, x')$ , which will be explained in detail in the next subsection.

##### B. Kernel Learning

The GPR kernel  $k(x; x')$  encodes the prior knowledge of the Gaussian random field  $f(\mathbf{x})$  in an implicit manner, i.e., the function  $f(\mathbf{x})$  is not written in an explicit formula. This implicit characteristics allow more field configurations to occur, and thus lead to enhanced model expressibility. To further enable more model flexibility, we usually assume a tunable kernel  $k(x; x'|\theta)$  with  $\theta \in \Theta \subset \mathbb{R}^n$  being a tunable hyperparameter. By tuning this hyperparameter, the model is better fit to the observed data, and thus the prediction quality can be further improved. The procedure of finding the optimal hyperparameter is termed as *kernel learning*.

Before finding the hyperparameter  $\theta$ , we must specify a criterion that evaluates which parameter is “better”, given the observed data. Usually, the ML criterion is applied, i.e.,

$$\hat{\theta}^{\text{ML}} = \arg \max_{\theta \in \Theta} \log p(\mathbf{y}|\theta), \quad (21)$$

where the probability density function  $p(\cdot|\theta)$  is given by

$$p(\mathbf{y}|\theta) = \frac{1}{\pi^N \det \mathbf{C}_\mathbf{y}} \exp(-\mathbf{y}^H \mathbf{C}_\mathbf{y}^{-1} \mathbf{y}). \quad (22)$$

Note that  $\mathbf{C}_\mathbf{y} = \mathbf{C}_\mathbf{y}(\theta)$  is a function of the hyperparameter. In order to obtain the ML estimator  $\hat{\theta}^{\text{ML}}$ , we need to compute the derivative of the log likelihood function  $\ell(\theta|\mathbf{y}) := \log p(\mathbf{y}|\theta)$  with respect to its hyperparameter  $\theta$ , and this derivative is expressed as

$$\begin{aligned} \frac{\partial \ell(\theta|\mathbf{y})}{\partial \theta_i} &= \frac{\partial}{\partial \theta_i} (-\mathbf{y}^H \mathbf{C}_\mathbf{y}^{-1} \mathbf{y} - \log \det \mathbf{C}_\mathbf{y}) \\ &= \boldsymbol{\alpha}^H \frac{\partial \mathbf{C}_\mathbf{y}}{\partial \theta_i} \boldsymbol{\alpha} - \text{tr} \left( \mathbf{C}_\mathbf{y}^{-1} \frac{\partial \mathbf{C}_\mathbf{y}}{\partial \theta_i} \right) \\ &= \text{tr} \left( (\boldsymbol{\alpha} \boldsymbol{\alpha}^H - \mathbf{C}_\mathbf{y}^{-1}) \frac{\partial \mathbf{C}_\mathbf{y}}{\partial \theta_i} \right) \end{aligned} \quad (23)$$

where  $\boldsymbol{\alpha} = \mathbf{C}_\mathbf{y}^{-1} \mathbf{y}$ , and  $i = 1, 2, \dots, n$  for each component  $\theta_i$  of the hyperparameter  $\theta$ . Note that the above formula is only valid for real hyperparameters  $\theta \in \mathbb{R}^n$ . For complex hyperparameters, the derivatives  $\partial/\partial \theta_i$  is replaced by Wirtinger derivatives  $(\partial/\partial \theta_{i,\text{Re}} - i\partial/\partial \theta_{i,\text{Im}})/2$  [39], and the derivative formula (23) remains unchanged due to the analyticity of  $\ell$  w.r.t. the elements of  $\mathbf{C}_\mathbf{y}$ . Any gradient-based optimizer can be applied to obtain an approximation of  $\hat{\theta}^{\text{ML}}$ . Unfortunately, for most forms of the kernel  $k(x; x'|\theta)$ , the entry of the matrix  $[\mathbf{C}_\mathbf{y}]_{jk} = k(x_j, x_k) + \sigma_\epsilon^2 \delta_{jk}$  is not a convex function of  $\theta_i$ . Thus, generally speaking, the global optimality of a gradient optimizer applied to  $\ell(\theta|\mathbf{y})$  is not guaranteed.

### C. Proposed EIT-GPR Channel Inference Algorithm

We assume the BS is equipped with  $N_{\text{BS}}$  antennas placing at  $\{\mathbf{d}_n\} \subset V_{\text{BS}} \subset \mathbb{R}^3, n \in [N_{\text{BS}}]$ , where  $V_{\text{Tx}}$  is the spatial region that encloses the BS transmitter. The uplink channel is snapshot at time  $t_p, p \in [P]$ , with  $P$  being the number of temporal snapshots. Following the GPR model, we can write the spacetime correlation tensor  $\mathbf{R}$  between the  $i$ -th polarization at the  $m$ -th antenna and the  $j$ -th polarization at the  $n$ -th antenna as

$$\mathbf{R}_{mn,pq,ij} = \mathbf{p}_i^T [\mathbf{K}_{\text{EM}}(\mathbf{d}_m, t_p; \mathbf{d}_n, t_q)] \mathbf{p}_j, \quad (24)$$

where  $\mathbf{p}_i \in \mathbb{R}^3$  is the polarization direction of the antenna,  $i, j \in [3]$ , and  $\mathbf{R}$  is a tensor with six indices. Although the correlation tensor  $\mathbf{R}$  seems complicated, it contains various symmetric properties. One can verify that by performing the following index exchanges, the tensor component is conjugated:

$$p \leftrightarrow q, m \leftrightarrow n, i \leftrightarrow j. \quad (25)$$

Since the indices  $(m, p, i)$  and  $(n, q, j)$  always appear together, we introduce the compound index  $\alpha = (m, p, i)$  and  $\beta = (n, q, j)$  for notation clarity. With this notation, the displacement vectors  $\mathbf{d}_m, \mathbf{d}_n$  are replaced by  $\mathbf{d}_\alpha, \mathbf{d}_\beta$ , and similar notation convention is applied to time instants  $t$  and polarization vectors  $\mathbf{p}$ .

The channel inference algorithm that takes in noisy channel observations and gives out estimated channel coefficient at arbitrary spatio-temporal coordinates is summarized in **Algorithm 1**. The key idea of this algorithm is to treat the unknown channel as a GRF, and then prediction can be performed by applying GPR. The algorithm framework is based on the computation of the posterior mean (19).

### D. EIT Kernel Learning

In order to further improve the fixed-kernel EIT-GPR channel inference routine in **Algorithm 1**, the problem of kernel learning remains to be solved. As is explained in Section IV-B, traditional GPR kernel learning requires evaluating the derivatives of the kernel value w.r.t. the hyperparameters. As for the EM kernel, the kernel value is given by  $\mathbf{p}_\alpha^T \mathbf{K}_{\text{EM}} \mathbf{p}_\beta$ , and the hyperparameters are the concentration parameter  $\boldsymbol{\mu}$ , the channel variance  $\sigma^2$ , and the Doppler velocity  $\mathbf{v}$ . Generally speaking, the EM kernel supports a spatio-temporal four-dimensional (4D) channel inference. However, in this paper, we only focus on the channel inference among spatial indices, i.e., MIMO channel estimation among multiple antennas. Thus, the hyperparameters are reduced to  $\boldsymbol{\mu}$  and  $\sigma^2$ . Further spatio-temporal 4D channel estimation and inference are left for future works.

The derivatives of the EM kernel w.r.t. the reduced hyperparameters are summarized in the following **Lemma 1**.

**Lemma 1** (Derivative of the EM kernel). *The Wirtinger derivative of  $\mathbf{K}_{\text{EM}}$  w.r.t.  $\boldsymbol{\mu}(k)$  and  $\sigma^2$  is given by*

$$\begin{aligned} \frac{\partial \mathbf{K}_{\text{EM}}}{\partial \boldsymbol{\mu}(k)} &= -\frac{\sigma^2}{C(\boldsymbol{\mu})} \left[ \mathbf{i} \frac{\partial \boldsymbol{\Sigma}(\mathbf{w})}{\partial \mathbf{w}(k)} + \frac{C'(\boldsymbol{\mu}) \boldsymbol{\mu}(k)}{C(\boldsymbol{\mu}) \boldsymbol{\mu}} \boldsymbol{\Sigma}(\mathbf{w}) \right], \\ \frac{\partial \mathbf{K}_{\text{EM}}}{\partial (\sigma^2)} &= \frac{1}{C(\boldsymbol{\mu})} \boldsymbol{\Sigma}(\mathbf{w}), \end{aligned} \quad (26)$$

### Algorithm 1 Proposed EIT-GPR Channel Inference Algorithm

**Input:** Hyperparameters  $\theta \in \Theta$ ; Received pilots  $y_\alpha, \alpha \in A$ ;

Noise variance  $\sigma_\epsilon^2$ ; Predictive spacetime indices  $\beta \in B$ .

**Output:** Estimated channel  $\hat{h}_\beta, \beta \in B$ .

1: # Stage 1 (EIT Kernel Generation):

2: Let  $\mathbf{K} \in \mathbb{C}^{|A| \times |A|}, \mathbf{y} \in \mathbb{C}^{|A| \times 1}$ .

3: **for**  $\alpha \in A$  **do**

4:   **for**  $\alpha' \in A$  **do**

5:     Construct the EM kernel: Compute  $\mathbf{K}_{\alpha\alpha'} \leftarrow \mathbf{p}_\alpha^T \mathbf{K}_{\text{EM}}(\mathbf{x}_\alpha, t_\alpha; \mathbf{x}_{\alpha'}, t_{\alpha'} | \theta) \mathbf{p}_{\alpha'} + \sigma_\epsilon^2 \delta_{\alpha\alpha'}$  by (16).

6:   **end for**

7: **end for**

8:  $\mathbf{a} \leftarrow \mathbf{K}^{-1} \mathbf{y}$ .

9: # Stage 2 (GPR Prediction):

10: Let  $\mathbf{W} \in \mathbb{C}^{|B| \times |A|}$ .

11: **for**  $\beta \in B$  **do**

12:   **for**  $\alpha \in A$  **do**

13:      $\mathbf{W}_{\beta\alpha} \leftarrow \mathbf{p}_\beta^T \mathbf{K}_{\text{EM}}(\mathbf{x}_\beta, t_\beta; \mathbf{x}_\alpha, t_\alpha | \theta) \mathbf{p}_\alpha$  by (16).

14:   **end for**

15: **end for**

16: Channel reconstruction:  $\hat{\mathbf{h}} \leftarrow \mathbf{W} \mathbf{a}$ .

17: **return** Estimated channel  $\hat{\mathbf{h}}$ .

where  $\mathbf{w} = k_0 \mathbf{z}$ ,  $\mathbf{z} = (\mathbf{x}_\alpha - \mathbf{x}_\beta) - \mathbf{i} \boldsymbol{\mu} / k_0$ ,  $\boldsymbol{\mu} = \|\boldsymbol{\mu}\|$ , and

$$\begin{aligned} \frac{\partial \boldsymbol{\Sigma}(\mathbf{w})}{\partial \mathbf{w}(k)} &= \frac{1}{8} \left[ \mathbf{i} (f_1 + f_3) \hat{\mathbf{w}}(k) \mathbf{I}_3 + \mathbf{i} (f_1 - 3f_3) \hat{\mathbf{w}}(k) \hat{\mathbf{w}} \hat{\mathbf{w}}^T \right. \\ &\quad \left. + (f_0 - 3f_2) (\partial_k \hat{\mathbf{w}} \cdot \hat{\mathbf{w}}^T + \hat{\mathbf{w}} \cdot \partial_k \hat{\mathbf{w}}^T) \right]. \end{aligned} \quad (27)$$

Here, the symbol  $\hat{\mathbf{w}} = \mathbf{w} / |\mathbf{w}|$ .

*Proof:* Details are shown in **Appendix A**. ■

Notice that the goal of kernel learning is to fit the EIT kernel-defined GRF to the observed data  $\mathbf{y} \in \mathbb{C}^{|A| \times 1}$ . Before performing kernel learning, we first need to specify the marginal log likelihood function  $\ell(\theta | \mathbf{y})$  as the objective function. To enhance the expressibility of the model, we choose the mixed EM kernel to be the convex combination of multiple sub-kernels, i.e.,

$$k_{\text{EM,Mixed}}(x_\alpha; x_\beta | \theta) = \mathbf{p}_\alpha^T \left( \sum_{s=1}^S w_s \mathbf{K}_{\text{EM}}(x_\alpha; x_\beta | \theta_s) \right) \mathbf{p}_\beta, \quad (28)$$

where  $w_s \geq 0$  are the non-negative weights satisfying  $\sum_s w_s = 1$ , and  $\theta$  represents the collection of all the hyperparameters that contain  $S$  different hyperparameters  $\theta_s \in \Theta$ . In the mixed kernel case, following (23), the log likelihood



function  $\ell(\{\boldsymbol{\mu}_s\}_{s=1}^S|\mathbf{y})$  is expressed as

$$\begin{aligned}\ell(\{\boldsymbol{\mu}_s, w_s\}_{s=1}^S, \sigma^2|\mathbf{y}) &= \log p(\mathbf{y}|\{\boldsymbol{\mu}_s, w_s\}_{s=1}^S) \\ &= -\mathbf{y}^H \mathbf{K}_y^{-1} \mathbf{y} - \log \det \mathbf{K}_y \\ &\quad + \text{const},\end{aligned}\quad (29)$$

where  $\mathbf{K}_y = \mathbf{K}_h + \sigma_\epsilon^2 \mathbf{I}_{N_A} = \sum_s w_s \mathbf{K}_s + \sigma_\epsilon^2 \mathbf{I}_{N_A}$ ,  $N_A = |A|$ ,  $\mathbf{h} \in \mathbb{C}^{|A| \times 1}$  represents the noiseless true values of the channel, and

$$(\mathbf{K}_h)_{\alpha\beta} = k_{\text{EM,Mixed}}(x_\alpha; x_\beta|\boldsymbol{\theta}). \quad (30)$$

Notice that the objective function (29) is a function of  $\mathbf{K}_y$ , which is further a matrix-valued function of hyperparameters  $\boldsymbol{\theta} = (\{\boldsymbol{\mu}_s, w_s\}_{s=1}^S, \sigma^2) \subset \Theta$ . Since the latter derivative  $\partial \mathbf{K}_y / \partial \boldsymbol{\mu}_s(k)$  has been solved in **Lemma 1**, we only need to compute the Wirtinger derivative of  $\ell$  w.r.t.  $\mathbf{K}_h$ . This is given by the following formula

$$\frac{\partial \ell}{\partial \mathbf{K}_h} = (\mathbf{a} \mathbf{a}^H - (\mathbf{K}_y^{-1}))^*, \quad (31)$$

where  $\mathbf{a} = \mathbf{K}_y^{-1} \mathbf{y}$ . Combining (31) with the conclusion of **Lemma 1**, we arrive at the real-variable derivative as

$$\frac{\partial \ell}{\partial \boldsymbol{\mu}_s(k)} = 2w_s \Re \left[ \text{tr} \left( \frac{\partial \mathbf{K}_h}{\partial \boldsymbol{\mu}_s(k)} (\mathbf{a} \mathbf{a}^H - \mathbf{K}_y^{-1}) \right) \right], \quad (32)$$

and

$$\frac{\partial \ell}{\partial w_s} = 2\Re [\text{tr} (\mathbf{K}_s(\theta_s)(\mathbf{a} \mathbf{a}^H - \mathbf{K}_y^{-1}))], \quad (33)$$

which can be used to solve the following kernel learning problem with the ML criterion

$$\hat{\boldsymbol{\theta}}^{\text{ML}} = \arg \max_{\boldsymbol{\theta}} \ell(\mathbf{y}|\boldsymbol{\theta}). \quad (34)$$

Given the derivatives (32), the numerical optimizer can be chosen as gradient ascent, conjugate gradient ascent, or Armijo-Goldstein backtracking search [40]. Note that the two terms appearing in (29) represent the data fitness and model complexity, respectively. Thus, minimization of the objective  $\ell$  will automatically balance between the data fitness and model complexity.

The EIT kernel learning procedure is summarized in **Algorithm 2**, and its performance will be numerically evaluated in the next section. Since we suppress the temporal dimension for simplicity, the following simulation results are mainly focused on channel estimation tasks without temporal predictions. Time-domain channel inference is beyond the scope of this paper, and is left for future works.

## V. SIMULATION RESULTS

In this section, we will present detailed simulation results, demonstrating the efficiency of EM kernel learning, and the performance of the proposed EIT-GPR channel estimation algorithm.

### A. EM Kernel Learning

In this subsection, we verify the EM kernel learning algorithm by fitting the EM kernel to channel observations  $\mathbf{y}$ . Both the single-kernel and the bi-kernel case are studied, i.e.,  $S \in \{1, 2\}$ . The simulation settings are shown in Fig. (new

---

### Algorithm 2 EIT Mixed Kernel Learning

---

**Input:** Received pilots  $y_\alpha$ ,  $\alpha \in A$ ; Noise variance  $\sigma_\epsilon^2$ ; Number of mixed kernels  $S$ ; Maximum iteration number  $N_{\text{iter}}$ .

**Output:** Estimated hyperparameters  $\{\hat{\boldsymbol{\mu}}_s, \hat{w}_s\}_{s=1}^S, \hat{\sigma}^2$ .

- 1:  $\hat{\sigma}^2 \leftarrow 2 \sum_{\alpha \in A} |y_\alpha|^2 / (|A| \cdot (1 + \sigma_\epsilon^2))$ .
  - 2: Let  $\mathbf{K}_y \in \mathbb{C}^{|A| \times |A|}$ , and  $\mathbf{y} \in \mathbb{C}^{|A| \times 1}$  containing input data from  $y_\alpha, \alpha \in A$ .
  - 3: Set  $t \leftarrow 0$ , and initialize the hyperparameters  $\{\hat{\boldsymbol{\mu}}_s^{(0)}, \hat{w}_s^{(0)}\}_{s=1}^S$ .
  - 4: Initialize the learning rates of Armijo-Goldstein's optimizer.
  - 5: **for**  $t = 1, 2, \dots, N_{\text{iter}}$  **do**
  - 6: Construct the EM kernel  $\mathbf{K}_y$  from hyperparameters  $\{\hat{\boldsymbol{\mu}}_s^{(t-1)}, \hat{w}_s^{(t-1)}\}_{s=1}^S$  by (16) and (28).
  - 7:  $\mathbf{a} \leftarrow \mathbf{K}_{\text{EM}}^{-1} \mathbf{y}$ .
  - 8: **for**  $s = 1, 2, \dots, S$  **do**
  - 9: Compute  $\frac{\partial \ell}{\partial \boldsymbol{\mu}_s(k)}$ ,  $k = 1, 2, 3$  from (32).
  - 10: Update  $\boldsymbol{\mu}_s^{(t)}$  with  $\frac{\partial \ell}{\partial \boldsymbol{\mu}_s(k)}$  by Armijo-Goldstein's optimizer.
  - 11: **end for**
  - 12: **for**  $s = 1, 2, \dots, S$  **do**
  - 13: Compute  $\frac{\partial \ell}{\partial w_s}$  from (33).
  - 14: Update  $w_s^{(t)}$  with  $\frac{\partial \ell}{\partial w_s}$  by Armijo-Goldstein's optimizer.
  - 15: **end for**
  - 16: **end for**
  - 17: **return** Estimated hyperparameters  $\{\hat{\boldsymbol{\mu}}_s^{(N_{\text{iter}})}, \hat{w}_s^{(N_{\text{iter}})}\}_{s=1}^S$ , and  $\hat{\sigma}^2$ .
- 

figure, describing the relative position of the BS and UE). The carrier frequency is set to  $f_c = 3.5$  GHz, and the number of BS antennas is set to  $N_{\text{BS}} = 32$ . Since for channel estimation problems, the "evidence" set  $A$  coincides with the prediction set  $B$ , we have  $|A| = |B| = N_{\text{BS}}$ . The uplink channel is generated by (a) the geometric model with Friis transmission formula; (b) the SV model [41]; (c) the TR 38.901 model [20]. The geometric model produces channel vector  $\mathbf{h}$  by directly calculating the channel coefficient as

$$\mathbf{h}(n) = \frac{\lambda}{4\pi d_n} e^{ikd_n}, \quad n \in [N_{\text{BS}}], \quad (35)$$

where  $d_i$  is the geometric distance (in meters) from the  $i$ -th BS antenna to the user, and  $r = 1$  is the path loss exponent. Note that the positive phase shift, i.e.,  $+ikd_n$ , is in agreement with the physicists' convention [42] of Fourier transforms.

*Simulation setup.* The EM kernel fitting is studied by applying the geometric model (a) and tuning the kernel to

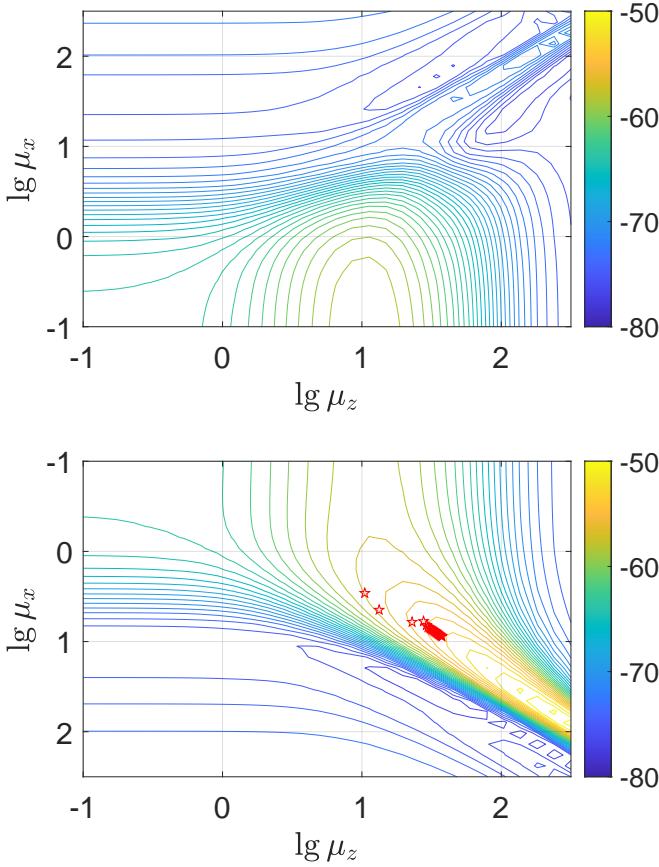


Fig. 3. GPR objective function  $\ln p(\mathbf{y}|\boldsymbol{\mu}_{x,z})$  and trajectory of the Armijo-Goldstein backtracking optimizer (in red pentagrams).

fit the channel observations  $\mathbf{y}$ . Fig. 3 shows the contour plot of the single-kernel GPR objective function  $\ell(\boldsymbol{\mu}_x, \boldsymbol{\mu}_z|\mathbf{y})$ . The variable  $\boldsymbol{\mu}_y$  is fixed to zero, since the user is assumed to be located in the  $xOz$  plane. During simulation,  $\varphi_{\text{UE}} = -15^\circ$ ,  $R_{\text{UE}} = 10$  m, and the receive SNR is set to be  $\gamma = 0$  dB. The user is intentionally placed in the near-field region of the BS array, in order to make the channel vector  $\mathbf{h}$  non DFT-like, i.e., the channel vector deviates from the far-field DFT channel. Although this non-DFT property prohibits traditional virtual channel-based angular analysis of the channel, this difficulty can be overcome by the proposed GPR channel fitter, since the EM kernel intrinsically supports multiple incoming waves.

*Kernel learning performance.* the objective function  $\ell(\boldsymbol{\mu}_x, \boldsymbol{\mu}_z|\mathbf{y})$  is drawn in two parts in Fig. 3. The upper half represents the objective function in the region  $\{\boldsymbol{\mu}_x > 0\}$ , and the lower half represents the objective function in the region  $\{\boldsymbol{\mu}_x < 0\}$ . For the sake of a broad functional vision, the variables are presented in log scale. The objective function attains better fitness at the lower half of the figure, and the region of better fitness extends in a ridge-shaped manner towards the southeast direction. In fact, this direction contains the information of the user's direction relative to the BS. Recall that the physical meaning of  $\boldsymbol{\mu}$  is the concentration parameter. Thus, in a nearly line-of-sight propagation environment, the

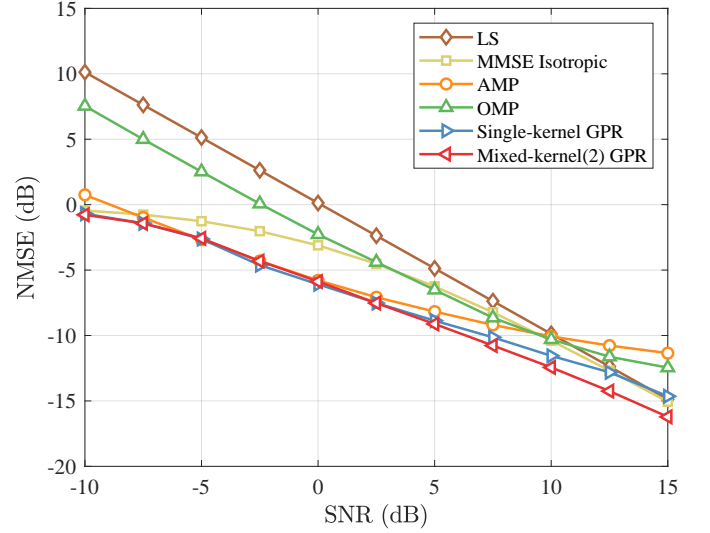


Fig. 4. GPR-based channel estimation with EM kernel and SV channel.

user's direction (azimuth) angle  $\varphi_{\text{UE}}$  satisfies

$$\tan \varphi_{\text{UE}} = \frac{\boldsymbol{\mu}_x}{\boldsymbol{\mu}_z}. \quad (36)$$

By applying the log transform, we obtain  $\lg |\boldsymbol{\mu}_x| = \lg |\tan \varphi_{\text{UE}}| + \lg |\boldsymbol{\mu}_z|$ , meaning that the intercept of the ridge corresponds to the angular-related quantity  $\lg \tan \varphi_{\text{UE}}$ . A coarse estimation of the interception produces  $\lg |\tan \varphi_{\text{UE}}| \approx 0.6$ , which yields  $\hat{\varphi}_{\text{UE}} \approx -14^\circ$ . The accuracy of this estimation demonstrates the correctness of the proposed EIT kernel and the GPR-based kernel learning algorithms.

#### B. GPR Channel Estimation with EM kernel

In the previous Section IV-D, we have proposed a channel inference algorithm that exploits the prior knowledge of the EM kernel. Although **Algorithm 1** and **Algorithm 2** are general, we apply them to the channel estimation task where the temporal variable  $t$  is suppressed. Further applications that extend to channel prediction and space-time channel interpolation tasks are left for future works.

*Simulation setup.* In the following channel estimation simulation, to ensure a more realistic channel property, we adopt (b) the standard SV multi-path synthetic channel model and (c) the standard 3GPP TR 38.901 CDL channel [20] for algorithm performance evaluation. For the multi-path SV model, the number of NLoS paths is set to  $L = 6$ , and the Rician factor is  $K = 10$  dB. The SV channel coefficients are normalized to ensure that  $\mathbb{E}[\|\mathbf{h}\|^2] = N_{\text{BS}}$ . The SV LoS path is generated according to the geometric AoA, i.e., the physical angular direction  $\varphi_{\text{UE}}$  of the user, and the NLoS path AoAs are uniformly generated within range  $[-\pi/2, \pi/2]$ .

*Baseline algorithms.* In Fig. 4, the proposed GPR estimators are compared with various baseline channel estimators under SV channel model. Fig. 5 presents the results under the standard CDL channel model. The LS estimator is given by  $\hat{\mathbf{h}}^{\text{LS}} = \mathbf{y}$ . The MMSE-isotropic estimator is constructed by

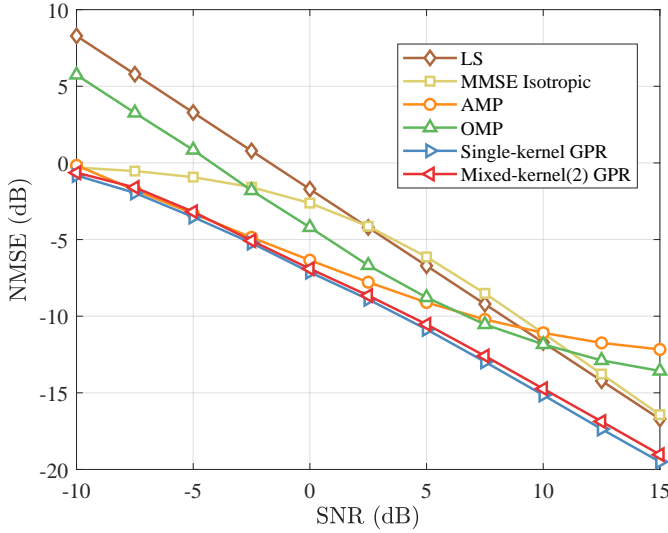


Fig. 5. GPR-based channel estimation with EM kernel and CDL channel.

setting the MMSE correlation matrix  $\mathbf{R} = \mathbf{K}_{\text{iso}}$  [43, Eqn.(8)] as

$$[\mathbf{K}_{\text{iso}}]_{\alpha\beta} = \sigma^2 \text{sinc}\left(\frac{2}{\lambda} \|\mathbf{x}_\alpha - \mathbf{x}_\beta\|\right). \quad (37)$$

Since the generated multi-path channel exhibits angular sparsity, compressed sensing (CS) algorithms can be applied to exploit this sparse property, and thus achieve high-quality channel estimation. In the simulation, we choose two CS algorithms as baselines, namely the approximate message passing (AMP) algorithm and the orthogonal matching pursuit (OMP) algorithm. The AMP algorithm is implemented according to [44] with shrinkage parameter  $\lambda = 1.2$ , and the OMP algorithm [45] is implemented with the number of path  $L + 1 = 7$ , matching the SV channel generation procedure. All the channel estimation algorithms are evaluated by the normalized mean square error (NMSE) performance, which is defined as

$$\text{NMSE} = \mathbb{E} \left[ \frac{\|\hat{\mathbf{h}} - \mathbf{h}\|^2}{\|\mathbf{h}\|^2} \right], \quad (38)$$

where the expectation  $\mathbb{E}[\cdot]$  is calculated by Monte-Carlo simulations.

*The proposed EIT-GPR method.* Simulation results in Fig. 4 and Fig. 5 have demonstrated that, both the proposed single-kernel GPR and the multi-kernel GPR methods can outperform the baseline algorithms in terms of normalized mean square error (NMSE) across an SNR range of  $-10 \sim 15$  dB. The mixed-kernel GPR method outperforms all its rivals, mainly due to its strongest capability to match the EM correlation laws in the received pilots. The single-kernel GPR method is superior to all the non-GPR methods, which demonstrates that the proposed EIT kernel better captures the fundamental laws of the EM channel. In other words, the EIT kernel provides better understandings of the wireless channel compared with the sparsity understanding in the AMP and OMP algorithms, and the isotropic fading understanding in the MMSE-isotropic algorithm [43]. Note that under both the SV channel model

and the CDL channel model, the proposed EIT-GPR methods outperform the baselines. However, the mixed-kernel GPR method does not always achieve the best performance, which is mainly due to over-parameterization brought by different channel statistics.

## VI. CONCLUSION

In this paper, we improve uplink channel estimators by exploiting the side information provided by EIT, thus proving that EIT is of great application value. Specifically, by leveraging the autocorrelation modelling methods in EIT, the correlated fading properties of the physical channel are accurately captured by a spatio-temporal correlation function called the EM kernel. Then, we propose an EIT-GPR channel estimation algorithm to exploit the side information contained in the EM kernel. Furthermore, due to the favorable analytic properties of the EM kernel, we propose a kernel learning approach to fit the EM kernel to the observed channel coefficients. This kernel learning approach refines the performance of EIT-GPR, making it possible to outperform traditional channel estimators. Finally, we test the proposed EIT-GPR estimator in uplink channel estimation with both SV and CDL channel models, achieving improved performance over traditional MMSE and CS-based channel estimators.

For future works, Doppler features can be extracted by tuning the EM kernel to fit the time-varying channel, thus enabling the application of the EM kernel to accurate channel prediction, fast channel tracking, and improved channel interpolation/extrapolation.

## APPENDIX A PROOF OF LEMMA 1

Since  $\sigma^2$  is only a multiplicative factor in (16), the derivative w.r.t.  $\sigma^2$  is easy to obtain. Thus, following (15), we focus on evaluating the derivative of  $\Sigma(\mathbf{w})$  w.r.t.  $\mathbf{w}$ . We notice that  $\Sigma(\mathbf{w})$  is a matrix-valued function of the complex vector variable  $\mathbf{w}$ , and more importantly, each matrix element is a multi-variable *analytic function* of  $\mathbf{w}$ . Following standard analytic differential techniques and using the recurrence formula<sup>5</sup>  $f_n^{(k)}(\beta) = i^k f_{n+k}(\beta)$ , we arrive at

$$\begin{aligned} \frac{\partial \Sigma(\mathbf{w})}{\partial \mathbf{w}(k)} = & \frac{1}{8} [i(f_1 + f_3)\hat{\mathbf{w}}(k)\mathbf{I}_3 + i(f_1 - 3f_3)\hat{\mathbf{w}}(k)\hat{\mathbf{w}}\hat{\mathbf{w}}^T \\ & + (f_0 - 3f_2)(\partial_k \hat{\mathbf{w}} \cdot \hat{\mathbf{w}}^T + \hat{\mathbf{w}} \cdot \partial_k \hat{\mathbf{w}}^T)], \end{aligned} \quad (39)$$

where  $\partial_k := \partial/\partial \mathbf{w}(k)$ ,  $\partial_k \hat{\mathbf{w}} = |\mathbf{w}|^{-1}(\hat{\mathbf{e}}_k - (\hat{\mathbf{w}}(k)\hat{\mathbf{w}}))\hat{\mathbf{w}}$ , and all the functions  $f_n(\cdot)$  are evaluated at  $\beta = |\mathbf{w}|$ .  $\hat{\mathbf{e}}_k$  denotes the unit vector with the only “1” located at the  $k$ -th component. Notice that, usually in order to fully describe the derivative of a complex-valued function  $g(w)$  w.r.t. a complex argument  $w$ , two derivatives should be involved, i.e.,  $\partial g/\partial w$  and  $\partial g/\partial w^*$ . Fortunately, due to the analyticity of  $\Sigma(\mathbf{w})$ , we have

$$\frac{\partial \Sigma}{\partial \mathbf{w}_k^*} = \mathbf{O}. \quad (40)$$

<sup>5</sup>This can be verified by differentiating both sides of (11) with respect to  $\beta$ , and swapping the integral and the differential operators.

Combining (39) and (40), the Wirtinger derivative of  $\mathbf{K}_{\text{EM}}$  w.r.t.  $\mu(k)$  can be evaluated as

$$\frac{\partial \mathbf{K}_{\text{EM}}}{\partial \mu(k)} = \sigma^2 \left( \frac{-i}{C(\mu)} \frac{\partial \Sigma}{\partial \mathbf{w}(k)} - \frac{C'(\mu) \mu(k)}{C^2(\mu) \mu} \Sigma \right), \quad (41)$$

where  $C'(\mu) = \mu^{-2}(\mu \cosh(\mu) - \sinh(\mu))$ . This completes the proof.

## REFERENCES

- [1] M. H. Alsharif, A. H. Kelechi, M. A. Albream, S. A. Chaudhry, M. S. Zia, and S. Kim, "Sixth generation (6G) wireless networks: Vision, research activities, challenges and potential solutions," *Symmetry*, vol. 12, no. 4, p. 676, Apr. 2020.
- [2] E. Basar, M. Di Renzo, J. De Rosny, M. Debbah, M.-S. Alouini, and R. Zhang, "Wireless communications through reconfigurable intelligent surfaces," *IEEE access*, vol. 7, pp. 116 753–116 773, 2019.
- [3] H. Q. Ngo, A. Ashikhmin, H. Yang, E. G. Larsson, and T. L. Marzetta, "Cell-free massive MIMO versus small cells," *IEEE Trans. Wireless Commun.*, vol. 16, no. 3, pp. 1834–1850, Jan. 2017.
- [4] M. Cui, Z. Wu, Y. Lu, X. Wei, and L. Dai, "Near-field MIMO communications for 6G: Fundamentals, challenges, potentials, and future directions," *IEEE Comm. Mag.*, vol. 61, no. 1, pp. 40–46, Jan. 2022.
- [5] M. Chafii, L. Bariah, S. Muhaidat, and M. Debbah, "Twelve scientific challenges for 6G: Rethinking the foundations of communications theory," *IEEE Comm. Surveys Tut.*, Feb. 2023.
- [6] J. Zhu, Z. Wan, L. Dai, M. Debbah, and H. V. Poor, "Electromagnetic information theory: Fundamentals, modeling, applications, and open problems," arXiv preprint arXiv:2212.02882, Sep. 2022.
- [7] M. D. Migliore, "Horse (electromagnetics) is more important than horsemanship (information) for wireless transmission," *IEEE Trans. Antenna Propagat.*, vol. 67, no. 4, pp. 2046–2055, Dec. 2018.
- [8] S. Loyka, "On the relationship of information theory and electromagnetism," in *IEEE 6th Int. Symp. Electr. Compat. Electr. Ecology*. IEEE, Jun. 2005, pp. 100–104.
- [9] M. D. Migliore, "Who cares about the horse? A gentle introduction to information in electromagnetic theory [wireless corner]," *IEEE Antenna Propagat. Mag.*, vol. 62, no. 5, pp. 126–137, Oct. 2020.
- [10] O. Bucci and G. Franceschetti, "On the spatial bandwidth of scattered fields," *IEEE Trans. Antenna Propagat.*, vol. 35, no. 12, pp. 1445–1455, Dec. 1987.
- [11] O. M. Bucci and G. Franceschetti, "On the degrees of freedom of scattered fields," *IEEE Trans. Antenna Propagat.*, vol. 37, no. 7, pp. 918–926, Jul. 1989.
- [12] D. A. Miller, "Communicating with waves between volumes: evaluating orthogonal spatial channels and limits on coupling strengths," *Applied Optics*, vol. 39, no. 11, pp. 1681–1699, Nov. 2000.
- [13] F. K. Gruber and E. A. Marengo, "New aspects of electromagnetic information theory for wireless and antenna systems," *IEEE Trans. Antenna Propagat.*, vol. 56, no. 11, pp. 3470–3484, Nov. 2008.
- [14] M. A. Jensen and J. W. Wallace, "Capacity of the continuous-space electromagnetic channel," *IEEE Trans. Antenna Propagat.*, vol. 56, no. 2, pp. 524–531, Feb. 2008.
- [15] R. Li, D. Li, J. Ma, Z. Feng, L. Zhang, S. Tan, E. Wei, H. Chen, and E.-P. Li, "An electromagnetic information theory based model for efficient characterization of MIMO systems in complex space," *IEEE Trans. Antenna Propagat.*, vol. 71, no. 4, pp. 3497–3508, Jan. 2023.
- [16] A. Pizzo, L. Sanguinetti, and T. L. Marzetta, "Spatial characterization of electromagnetic random channels," *IEEE Open J. Comm. Soc.*, vol. 3, pp. 847–866, Apr. 2022.
- [17] A. Pizzo, T. L. Marzetta, and L. Sanguinetti, "Spatially-stationary model for holographic MIMO small-scale fading," *IEEE J. Sel. Areas Commun.*, vol. 38, no. 9, pp. 1964–1979, Sep. 2020.
- [18] A. Pizzo, L. Sanguinetti, and T. L. Marzetta, "Fourier plane-wave series expansion for holographic MIMO communications," *IEEE Trans. Wireless Commun.*, vol. 21, no. 9, pp. 6890–6905, Sep. 2022.
- [19] T. Wang, W. Han, Z. Zhong, J. Pang, G. Zhou, S. Wang, and Q. Li, "Electromagnetic-compliant channel modeling and performance evaluation for holographic MIMO," in *Proc. IEEE Globecom Workshops*. IEEE, Dec. 2022, pp. 747–752.
- [20] *Study on channel model for frequencies from 0.5 to 100 GHz (Release 16) v16.1.0*, 3GPP TR 38.901 TSG RAN; NR, Dec. 2019.
- [21] A. F. Molisch, H. Asplund, R. Heddergott, M. Steinbauer, and T. Zwick, "The COST259 directional channel model-part I: Overview and methodology," *IEEE Trans. Wireless Commun.*, vol. 5, no. 12, pp. 3421–3433, Dec. 2006.
- [22] J.-P. Kermoal, L. Schumacher, K. I. Pedersen, P. E. Mogensen, and F. Frederiksen, "A stochastic MIMO radio channel model with experimental validation," *IEEE J. Sel. Areas Commun.*, vol. 20, no. 6, pp. 1211–1226, Aug. 2002.
- [23] A. A. Saleh and R. Valenzuela, "A statistical model for indoor multipath propagation," *IEEE J. Sel. Areas Commun.*, vol. 5, no. 2, pp. 128–137, Feb. 1987.
- [24] T. Van Erven and P. Harremoës, "Rényi divergence and Kullback-Leibler divergence," *IEEE Trans. Inf. Theory*, vol. 60, no. 7, pp. 3797–3820, Jun. 2014.
- [25] A. Lapidot and S. Shamai, "Fading channels: how perfect need "perfect side information" be?" *IEEE Trans. Inf. Theory*, vol. 48, no. 5, pp. 1118–1134, May 2002.
- [26] T. Hesketh, R. C. de Lamare, and S. Wales, "Adaptive MMSE channel estimation algorithms for MIMO systems," in *Proc. 18th Euro. Wirel. Conf.* VDE, Apr. 2012, pp. 1–5.
- [27] C. K. Williams and C. E. Rasmussen, *Gaussian processes for machine learning*. MIT press Cambridge, MA, 2006.
- [28] S. L. Loyka, "Channel capacity of MIMO architecture using the exponential correlation matrix," *IEEE Comm. Lett.*, vol. 5, no. 9, pp. 369–371, Sep. 2001.
- [29] Z. Wan, J. Zhu, Z. Zhang, L. Dai, and C.-B. Chae, "Mutual information for electromagnetic information theory based on random fields," *IEEE Trans. Commun.*, vol. 71, no. 4, pp. 1982–1996, Apr. 2023.
- [30] L. Hormander, *An introduction to complex analysis in several variables*. Elsevier, 1973.
- [31] K. V. Mardia and S. El-Atoum, "Bayesian inference for the von Mises-Fisher distribution," *Biometrika*, vol. 63, no. 1, pp. 203–206, Apr. 1976.
- [32] L. V. Ahlfors, *Complex analysis*. AMS Chelsea Publishing, 1979.
- [33] L. Liu, H. Feng, T. Yang, and B. Hu, "MIMO-OFDM wireless channel prediction by exploiting spatial-temporal correlation," *IEEE Trans. Wireless Commun.*, vol. 13, no. 1, pp. 310–319, Dec. 2013.
- [34] W. C. Jakes, "Mobile microwave communication," 1974.
- [35] G. J. Byers and F. Takawira, "Spatially and temporally correlated MIMO channels: Modeling and capacity analysis," *IEEE Trans. Veh. Technol.*, vol. 53, no. 3, pp. 634–643, May 2004.
- [36] A. Abdi and M. Kaveh, "A versatile spatio-temporal correlation function for mobile fading channels with non-isotropic scattering," in *Proceedings of the Tenth IEEE Workshop on Statistical Signal and Array Processing (Cat. No. 00TH8496)*. IEEE, Aug. 2000, pp. 58–62.
- [37] T. M. Cover, *Elements of information theory*. John Wiley & Sons, 1999.
- [38] M. Wytock and Z. Kolter, "Sparse gaussian conditional random fields: Algorithms, theory, and application to energy forecasting," in *International conference on machine learning*. PMLR, Mar. 2013, pp. 1265–1273.
- [39] R. Remmert, *Theory of complex functions*. Springer Science & Business Media, 1991, vol. 122.
- [40] J. E. Dennis Jr and R. B. Schnabel, *Numerical methods for unconstrained optimization and nonlinear equations*. SIAM, 1996.
- [41] A. Meijerink and A. F. Molisch, "On the physical interpretation of the Saleh-Valenzuela model and the definition of its power delay profiles," *IEEE Trans. Antenna Propagat.*, vol. 62, no. 9, pp. 4780–4793, Jul. 2014.
- [42] J. L. Bauck, "A note on Fourier transform conventions used in wave analyses," *EngrXiv.org*, Jul. 2018.
- [43] Ö. T. Demir, E. Björnson, and L. Sanguinetti, "Channel modeling and channel estimation for holographic massive MIMO with planar arrays," *IEEE Wirel. Commun. Lett.*, vol. 11, no. 5, pp. 997–1001, May 2022.
- [44] D. L. Donoho, A. Maleki, and A. Montanari, "Message passing algorithms for compressed sensing: I. motivation and construction," in *Proc. IEEE Inf. Theory Workshop (ITW'10)*. IEEE, Jul. 2010, pp. 1–5.
- [45] T. T. Do, L. Gan, N. Nguyen, and T. D. Tran, "Sparsity adaptive matching pursuit algorithm for practical compressed sensing," in *Proc. 42nd Asilomar Conf. Sig. Systems Comput.* IEEE, Oct. 2008, pp. 581–587.